Supplementary information

Novel suppression strategy of mid-spatial-frequency errors in sub-aperture polishing: adaptive spacing-swing controllable spiral magnetorheological finishing (CSMRF) method

Bo Wang[1,2,3], Feng Shi[1,2,3*], Ci Song[1,2,3*], Ping Zhou[4], Xing Peng[1,2,3], Qing Gao[5,6] Shuo Qiao[1,2,3], Guipeng Tie[1,2,3], Wanli Zhang[1,2,3], Ye Tian[1,2,3], Dede Zhai[1,2,3], Qun Hao[5,6,7]

[1] College of Intelligence Science and Technology, National University of Defense Technology, 109 Deya Road, Changsha 410073, China.
[2] National Key Laboratory of Equipment State Sensing and Smart Support, Changsha, Hunan 410073, China.
[3] Hunan Key Laboratory of Ultra-Precision Machining Technology, Changsha 410073, China.
[4] State Key Laboratory of High-performance Precision Manufacturing, Dalian University of Technology, Dalian 116024, China.

[5] National Key Laboratory on Near-surface Detection, Beijing, 100072, China.

[6] School of Optics and Photonics, Beijing Institute of Technology, Beijing 100081, China.
[7] Physics Department, Changchun University of Science and Technology, Changchun 130022, China.

***shifeng@nudt.edu.cn**

***songci@nudt.edu.cn**

High-performance, non-negative gradient constraint dwell-time solution algorithm based on the Lagrange regularization method

We employed a dwell-time solving algorithm rooted in the linear equation model to tackle the problem of a time-varying TIF relative to the machining position. By integrating the fundamental concept with the non-rotational symmetry characteristics of the controllable spiral magnetorheological polishing TIF, the following linear system of equations was established:

Figure S1 is a schematic diagram of the discrete grid division of the linear equations model. As shown in Figure S1, the initial surface error is divided into discrete grids, and a series of surface error control points $p_i(x_i, y_i)$ can be obtained, where the coordinates of the its surface shape error control point is (x_i, y_i). The surface error value corresponding to this point is h_i and we define the control area as a_i according to a certain area division rule. The dwell position of the TIF in the figuring process is defined as dwell point $l_k(x_k, y_k)$, where the dwell time at the j dwell point is t_j. The surface shape error control point vector is defined as $\vec{P} = [p_1, \cdots, p_i, \cdots, p_m]^T$, the surface shape error value vector is $\vec{H} = [h_1, \cdots, h_i, \cdots, h_m]^T$, the dwell point vector is $\vec{L} = [l_1, \cdots, l_k, \cdots, l_n]^T$, and the dwell time vector is $\vec{T} = [t_1, \cdots, t_j, \cdots, t_n]^T$.

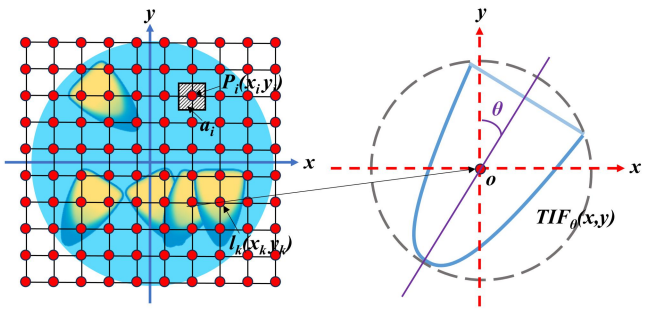

Figure S1 The diagram of discrete grid division of linear equations model

We define the removal vector as $\overrightarrow{F^k}=[F_1^k,\cdots,F_i^k,\cdots,F_m{}^k]^T$. This represents the amount of material removed at each surface-shape-error control point when the TIF is located at the dwell point l_k. The removal efficiency F_i^k at each surface shape error control point p_i is

$$F_i^k=\frac{1}{a_i}\iint_{S_{in}} TIF_\theta(x,y)\cdot dxdy \tag{S1}$$

where $TIF_\theta(x,y)$ represents the spiral TIF at different positions and S_{in} is the area where the control area a_i is inside the TIF. When the surface error control point p_i is located outside TIF, $F_i^k=0$.

We define the removal matrix $F_{m\times n}=[\vec{F}^1,\cdots,\vec{F}^k,\cdots,\vec{F}^n]$ as follows:

$$F_{m\times n}=\begin{bmatrix} F_1^1 & F_1^2 & \cdots & F_1^j & \cdots & F_1^n \\ F_2^1 & F_2^2 & \cdots & F_2^j & \cdots & F_2^n \\ \vdots & \vdots & \ddots & \vdots & \ddots & \vdots \\ F_i^1 & F_i^2 & \cdots & F_i^j & \cdots & F_i^n \\ \vdots & \vdots & \ddots & \vdots & \ddots & \vdots \\ F_m{}^1 & F_m{}^2 & \cdots & F_m{}^j & \cdots & F_m{}^n \end{bmatrix} \tag{S2}$$

The amount of material removed due to the surface shape error is the sum of the products of the unit material removal amount and the dwell time at each surface shape error control point. Consequently, the process of determining dwell time transforms into an inverse problem of solving the large sparse matrix equations presented below:

$$\begin{bmatrix} F_1^1 & F_1^2 & \cdots & F_1^j & \cdots & F_1^n \\ F_2^1 & F_2^2 & \cdots & F_2^j & \cdots & F_2^n \\ \vdots & \vdots & \ddots & \vdots & \ddots & \vdots \\ F_i^1 & F_i^2 & \cdots & F_i^j & \cdots & F_i^n \\ \vdots & \vdots & \ddots & \vdots & \ddots & \vdots \\ F_m{}^1 & F_m{}^2 & \cdots & F_m{}^j & \cdots & F_m{}^n \end{bmatrix}\cdot\begin{bmatrix} t_1 \\ t_2 \\ \vdots \\ t_j \\ \vdots \\ t_n \end{bmatrix}=\begin{bmatrix} h_1 \\ h_2 \\ \vdots \\ h_i \\ \vdots \\ h_m \end{bmatrix} \tag{S3}$$

The final machining residual error is shown in (S4), which is the surface shape error after error correction of the controllable spiral magnetorheological polishing.

$$res = H - F_{m\times n} \cdot T \tag{S4}$$

In this study, we employed the lsqlin function to solve large sparse linear matrix equation problems and obtain constrained nonnegative solutions [33, 34]. This method ensures that the calculated dwell times exceed the minimum dwell time achievable based on the machine tool speeds. The lsqlin function utilizes a constrained linear least-squares algorithm, with the iteration process grounded in a preconditioned conjugate gradient method. The initial point for lsqlin was set to 1, with an upper limit of 4 and a lower limit of 0.02, ensuring compliance with the speed requirements for machine tool motion.

However, because the existing removal matrix is a severely ill-conditioned large sparse matrix, when the removal matrix $F_{m\times n}$ is ill-conditioned with a very large condition number, any small error is amplified in the dwell-time results, leading to non-smooth solutions. The change in spatial posture of the TIF at different dwell points in the controllable spiral TIF causes the removal matrix $F_{m\times n}$ to become "disordered," resulting in poorer smoothness of the dwell time under the current dwell time solving methods. The existing lsqlin function solves the dwell-time model while minimizing residual error during the solution process. However, in actual machine tool operations, the dwell-time implementation model must convert dwell time into a precise and smoothly achievable dwell speed. This means that the dwell time distribution should be continuous and smooth. A common approach to address this issue is to incorporate a regularization term. In our algorithm, we introduced a Laplacian regularization term. The Laplacian operator is a second-order differential operator primarily employed in image processing for tasks such as image enhancement and edge detection, among other applications. The Laplacian transformation of a typical binary function is defined as:

$$\nabla^2 f = \frac{\partial^2 f}{\partial x^2} + \frac{\partial^2 f}{\partial y^2} \tag{S5}$$

For ease of discrete processing, the Laplacian operator is generally expressed in the discrete form:

$$\nabla^2 f = [f(x+1,y)+f(x-1,y)+f(x,y+1)+f(x,y-1)]-4\cdot f(x,y) \quad \text{(S6)}$$

The Laplace operator effectively characterizes the gradient distribution features of a function. Incorporating it into the dwell time solving process allows for gradient constraints on the dwell time. By introducing dwell-time gradient control parameters and utilizing a specific operator, a smoother and more stable solution for dwell time can be achieved. By seeking a dwell time solution with a smooth gradient within the dwell time distribution domain, we ultimately obtain a dwell time distribution that meets high dynamic requirements.

Based on the discrete form of the Laplace operator, we adopted the template form of the Laplace operator and chose the template L as follows:

$$L = \begin{bmatrix} 0 & 1 & 0 \\ 1 & -4 & 1 \\ 0 & 1 & 0 \end{bmatrix} \quad \text{(S7)}$$

The original lsqlin function solves the least-squares algorithm with the objective of minimizing the L2 norm of the residuals, as shown in Equation (S8). However, the objective function is enhanced by incorporating a Laplacian operator, as indicated in Equation (S9), where LL represents the regularization factor. Furthermore, by adding dwell-time gradient constraint conditions to the model, we achieve a highly dynamic dwell-time framework. Mathematically, this model can be expressed as a constrained optimization problem in Equation (S10). By integrating the dwell time gradient constraints, the lsqlin function balances the trade-off between the RMS surface shape error and smoothness during the solving process to determine the minimum value. Once the regularization parameter is established and the preset convergence accuracy is achieved, the algorithm terminates.

$$Arg\min\{resnorm = \left\| F_{m\times n}\cdot T - H \right\|_2^2 : lb \le T \le ub\} \quad \text{(S8)}$$

$$Arg\min\{resnorm = \left\| F_{m\times n}\cdot T - H \right\|_2^2 + \lambda \left\| L\cdot T \right\|_2^2 : lb \le T \le ub\} \quad \text{(S9)}$$

$$\min_{lb \le x \le ub} \left\{ \left\| \left\| F_{m \times n} \cdot T - H \right\|_2^2 + \lambda \left\| L \cdot T \right\|_2^2 \right\| \right\} = \min_{lb \le x \le ub} \left\| \begin{bmatrix} F_{m \times n} \\ \sqrt{\lambda} \cdot L \end{bmatrix} \cdot T - \begin{bmatrix} H \\ 0 \end{bmatrix} \right\|^2 \tag{S10}$$